Monthly Notices
of the
ROYAL ASTRONOMICAL SOCIETY

MNRAS **480,** 2733–2742 (2018)
Advance Access publication 2018 August 6

doi:10.1093/mnras/sty1996

Discovery of a radio galaxy at $z = 5.72$

A. Saxena,[1]★ M. Marinello,[1,2] R. A. Overzier,[2] P. N. Best,[3] H. J. A. Röttgering,[1] K. J. Duncan,[1] I. Prandoni,[4] L. Pentericci,[5] M. Magliocchetti,[6] D. Paris,[5] F. Cusano,[7] F. Marchi,[5] H. T. Intema[1] and G.K. Miley[1]

[1]*Leiden Observatory, Leiden University, PO Box 9513, NL-2300 RA Leiden, the Netherlands*
[2]*Observatório Nacional, Rua General José Cristino, 77, São Cristóvão, Rio de Janeiro, RJ, CEP 20921-400, Brazil*
[3]*Institute for Astronomy, University of Edinburgh, Royal Observatory, Blackford Hill, EH9 3HJ Edinburgh, UK*
[4]*INAF-Instituto di Radioastronomia, Via P. Gobetti 101, I-40129 Bologna, Italy*
[5]*INAF-Osservatorio Astronomico di Roma, Via Frascati 33, I-00040 Monteporzio (RM), Italy*
[6]*IAPS-INAF, Via Fosso del Cavaliere 100, I-00133 Rome, Italy*
[7]*INAF-Osservatorio di Astrofisica e Scienza dello Spazio di Bologna, Via P. Gobetti 93/3, I-40129 Bologna, Italy*

Accepted 2018 July 12. Received 2018 July 05; in original form 2018 June 4

ABSTRACT

We report the discovery of the most distant radio galaxy to date, TGSS J1530+1049 at a redshift of $z = 5.72$, close to the presumed end of the Epoch of Reionization. The radio galaxy was selected from the TGSS ADR1 survey at 150 MHz for having an ultra-steep spectral index, $\alpha^{150\,\mathrm{MHz}}_{1.4\,\mathrm{GHz}} = -1.4$ and a compact morphology obtained using VLA imaging at 1.4 GHz. No optical or infrared counterparts for the radio source were found in publicly available sky surveys. Follow-up optical spectroscopy at the radio position using GMOS on Gemini North revealed the presence of a single emission line. We identify this line as Lyman alpha at $z = 5.72$, because of its asymmetric line profile, the absence of other optical/UV lines in the spectrum, and a high equivalent width. With an Lyα luminosity of 5.7×10^{42} erg s^{-1} and an FWHM of 370 km s^{-1}, TGSS J1530+1049 is comparable to 'non-radio' Lyman alpha emitters (LAEs) at a similar redshift. However, with a radio luminosity of $\log L_{150\mathrm{MHz}} = 29.1$ W Hz^{-1} and a deconvolved physical size 3.5 kpc, its radio properties are similar to other known radio galaxies at $z > 4$. Subsequent J and K band imaging using LUCI on the Large Binocular Telescope resulted in non-detection of the host galaxy down to 3σ limits of $J > 24.4$ and $K > 22.4$ (Vega). The K band limit is consistent with $z > 5$ from the $K - z$ relation for radio galaxies and helps rule out low redshifts. The stellar mass limit derived using simple stellar population models is $M_{\mathrm{stars}} < 10^{10.5}$ M$_\odot$. Its relatively low stellar mass and small radio and Lyα sizes suggest that TGSS J1530+1049 may be a radio galaxy in an early phase of its evolution.

Key words: galaxies: high-redshift – galaxies: individual: TGSS J1530+1049.

1 INTRODUCTION

High-redshift radio galaxies (HzRGs) are thought to be the progenitors of local massive elliptical galaxies and generally contain large amounts of dust and gas (Best et al. 1998; Carilli et al. 2002a; Reuland et al. 2004; De Breuck et al. 2010). They are also among the most massive galaxies at their redshift (Overzier et al. 2009) and are often found to be located at the centre of clusters and proto-clusters of galaxies (Pentericci et al. 2000; Venemans et al. 2002; Röttgering et al. 2003; Miley et al. 2004; Hatch et al. 2011; Orsi et al. 2016). Studies of their environment can give insights into the assembly and evolution of the large-scale structure in the Universe. Miley & De Breuck (2008) provide an extensive review about the properties of distant radio galaxies and their environments.

Radio galaxies at $z > 6$, in the Epoch of Reionization (EoR), are of particular interest as they could be used as unique tools to study the process of reionization in detail. At these redshifts, the hyper-fine transition line from neutral hydrogen atoms, with a rest-frame wavelength of 21 cm, falls in the low-frequency radio regime and can be observed as absorption signals in spectra of luminous background radio sources such as radio galaxies (Carilli, Gnedin & Owen 2002b; Furlanetto & Loeb 2002; Xu et al. 2009; Mack & Wyithe 2012; Ewall-Wice et al. 2014; Ciardi et al. 2015). Such 21-cm absorption signals from patches of neutral hydrogen clouds in the early Universe could, in principle, be observed by current and next-generation radio telescopes such as the Giant Metre-wave Radio Telescope (GMRT; Swarup et al. 1991), the Low-Frequency

★ E-mail: saxena@strw.leidenuniv.nl

© 2018 The Author(s)
Published by Oxford University Press on behalf of the Royal Astronomical Society

Downloaded from https://academic.oup.com/mnras/article-abstract/480/2/2733/5067277 by Royal Observatory Library user on 03 October 2018

Array (LOFAR; van Haarlem et al. 2013), the Murchinson Widefield Array (MWA; Tingay et al. 2013), and the Square Kilometer Array (SKA; Dewdney et al. 2009). This unique application motivates searches for bright-enough radio galaxies at the highest redshifts from deep all-sky surveys at low radio frequencies.

Finding powerful radio galaxies at increasingly large distances or redshifts, however, is challenging. HzRGs, which are rare and flux-limited samples, have shown that their space densities fall off dramatically at $z > 2 - 3$ (Dunlop & Peacock 1990; Willott et al. 2001; Rigby et al. 2011, 2015). Although a number of quasars at $z > 5$ are known, with a few also being radio-loud (see Bañados et al. 2015, for example), especially the recently discovered powerful radio quasar at $z = 5.84$ (Bañados et al. 2018; Momjian et al. 2018), the same cannot be said for radio galaxies – previously, the only known radio galaxy at $z > 5$ was TN J0924 − 2201 at $z = 5.19$ (van Breugel et al. 1999). If the orientation-based unification of radio galaxies and quasars is valid (see Morabito et al. 2017, for example), the number of radio quasars and galaxies at any given epoch should be comparable and it may be possible that many of the already unidentified radio sources are at $z > 5$. The scarcity of $z > 5$ radio galaxies could therefore be due to the relative difficulty in first identifying these sources amongst the wider radio source population, and then obtaining spectroscopic redshifts for these radio galaxies, which are optically much fainter than quasars. Dedicated spectroscopic follow-up of radio sources such as the WEAVE-LOFAR survey (Smith et al. 2016), and the upcoming major optical facilities such as the Extremely Large Telescope (ELT), the Thirty Meter Telescope (TMT), the Giant Magellan Telescope (GMT), and the James Webb Space Telescope (JWST) will help overcome these difficulties and potentially help characterize a number of USS radio sources.

The key requirement for gathering enough statistics for meaningful studies of radio galaxies at high-redshifts are deep low-frequency radio surveys covering large areas on the sky. Surveys such as the TIFR GMRT Sky Survey Alternative Data Release 1 (TGSS; Intema et al. 2017) and the currently ongoing surveys using LOFAR (Shimwell et al. 2017) are opening up new parameter spaces for searches for radio galaxies at $z \geq 6$. Using TGSS, which covers the entire radio sky north of −53 declination at a frequency of 150 MHz and achieving a median noise level of 3.5 mJy beam^{-1}, we launched a campaign to hunt for fainter and potentially more distant HzRGs, with the ultimate aim of discovering radio galaxies that could be suitable probes of the EoR (Saxena et al. 2018). In this paper, we report the discovery of a radio galaxy at a redshift of $z = 5.72$, TGSS J1530+1049, which was pre-selected as part of our sample of high-redshift radio galaxy candidates.

The layout of this paper is as follows. In Section 2, we present details about the initial source selection criteria and follow-up radio observations at high resolution for TGSS J1530+1049. In Section 3, we present the new optical spectroscopy and infrared imaging obtained for TGSS J1530+1049 and expand upon the data reduction methods. In Section 4, we describe how the redshift for this source was determined. In Section 5, we study the emission line and radio properties of this source and set constraints on its stellar mass. We also compare the observed properties to galaxies at the same epoch from the literature. Finally, in Section 6, we summarize the findings of this paper. Throughout this paper, we assume a flat ΛCDM cosmology with $H_0 = 70\,\mathrm{km\ s^{-1}\ Mpc^{-1}}$ and $\Omega_m = 0.3$. Using this cosmology, at a redshift of 5.72, the age of the Universe is 0.97 Gyr, and the angular scale per arcsecond is 5.86 kpc.

2 SOURCE SELECTION

Our two-stage selection process, based on first isolating compact radio sources with an ultra-steep spectrum (USS; $\alpha < -1.3$, where $S_\nu \propto \nu^\alpha$) at radio wavelengths, has historically been very successful at finding HzRGs from wide-area radio surveys (Röttgering et al. 1994; Blundell, Rawlings & Willott 1999; De Breuck et al. 2000; Afonso et al. 2011), and then combining it with optical and/or infrared faintness requirements. The relation that exists between the apparent K-band magnitude of radio galaxies and their redshift, known as the $K - z$ relation, (Lilly & Longair 1984; Jarvis et al. 2001; Willott et al. 2003; Rocca-Volmerange et al. 2004) gives further strength to the argument of selecting USS sources that are also faint at near-infrared wavelengths in a bid to isolate HzRGs (Ker et al. 2012). Deep near-infrared imaging of promising USS candidates can therefore serve as an independent way to set constraints on the redshifts of radio sources. HzRGs are expected to be very young and therefore, have small sizes at the highest redshifts (Saxena, Röttgering & Rigby 2017): implementing an additional criterion that puts an upper limit on the angular sizes of radio sources has the potential to increase the efficiency of pinpointing the highest redshift sources in a wide-area radio survey.

Combining all of these selection methods, we first shortlisted 588 candidates with an ultra-steep spectrum ($\alpha_{1.4\,\mathrm{GHz}}^{150\,\mathrm{MHz}} < -1.3$) and compact morphologies, out of a total of 65 996 sources that had spectral index information from TGSS and FIRST/NVSS. This sample probes fainter flux densities than previous large-area searches and has flux limits that ensure that a new parameter space in flux density and spectral index is probed, where a large number of undiscovered HzRGs are expected to lie (Ishwara-Chandra et al. 2010). From this shortlist, we then retained in our sample only those radio sources that are blank in all available optical surveys such as the Sloan Digital Sky Survey DR12 (SDSS; Alam et al. 2015) and the Pan-STARRS1 survey (PS1; Chambers et al. 2016), and infrared surveys such as ALLWISE using the *WISE* satellite (Wright et al. 2010) and the UKIDSS surveys (Lawrence et al. 2007) to maximize the chances of finding radio galaxies at the highest redshifts. This led to a final sample of 32 very promising HzRG candidates. Details of the sample selection can be found in Saxena et al. (2018).

High-resolution imaging using the Karl G. Jansky Very Large Array (VLA) for the 32 candidates, including for TGSS J1530+1049 (RA: 15:30:49.9, Dec: +10:49:31.1) is presented in Saxena et al. (2018), which was used to obtain morphologies and sub-arcsecond localization of the expected positions of the host galaxies, enabling blind spectroscopic follow-up. TGSS J1530+1049, in particular, showed a compact morphology, which was fitted with a single Gaussian. With a flux density of $S_{150\mathrm{MHz}} = 170 \pm 34$ mJy, TGSS J1530+1049 is one of the brightest sources in the sample. At 1.4 GHz, it has a flux density $S_{1.4\mathrm{GHz}} = 7.5 \pm 0.1$ mJy, giving a spectral index of $\alpha = -1.4 \pm 0.1$. With a relatively small (deconvolved) angular size of 0.6 ± 0.1 arcsec, TGSS J1530+1049 was deemed to be a promising HzRG candidate. We show the location of TGSS J1530+1049 in the flux density–spectral index parameter space in Fig. 1.

TGSS J1530+1049 is not detected in any of the PS1 bands (g, r, i, z, and y). This source also happens to lie in the sky area covered by the UKIDSS Large Area Survey (LAS), and is not detected down to (Vega) magnitude limits of $y > 20.5$, $J > 20.0$, $H > 18.8$, and $K > 18.4$. We show the image obtained from stacking all of the LAS bands with radio contours overlaid in Fig. 2. Lastly, this source is also not detected in any of the ALLWISE bands. These non-detections coupled with the ultra-steep radio spectral index and

Downloaded from https://academic.oup.com/mnras/article-abstract/480/2/2733/5067277 by Royal Observatory Library user on 03 October 2018

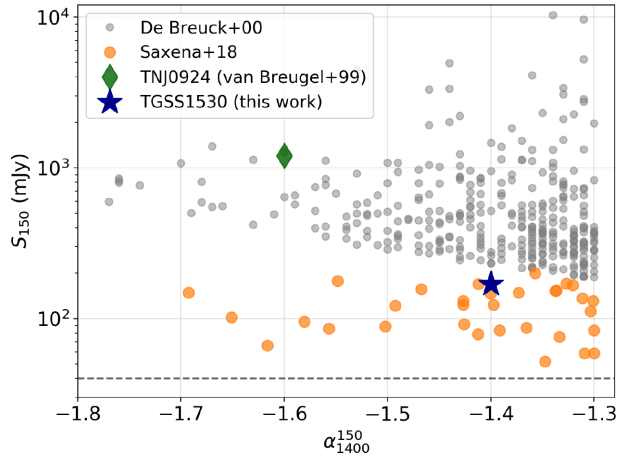

Figure 1. The location of TGSS J1530+1049 in the flux density–spectral index parameter space. The large orange points show the parameter space probed by the Saxena et al. (2018) sample and the smaller grey points show radio sources from De Breuck et al. (2000), scaled to an observed frequency of 150 MHz using the spectral indices provided for individual sources. Also shown for comparison is TN J0924 − 2201 at $z = 5.2$ (van Breugel et al. 1999). TGSS J1530+1049 is fainter than the previously studied large-area samples and offers a new window into fainter radio galaxies at high redshifts.

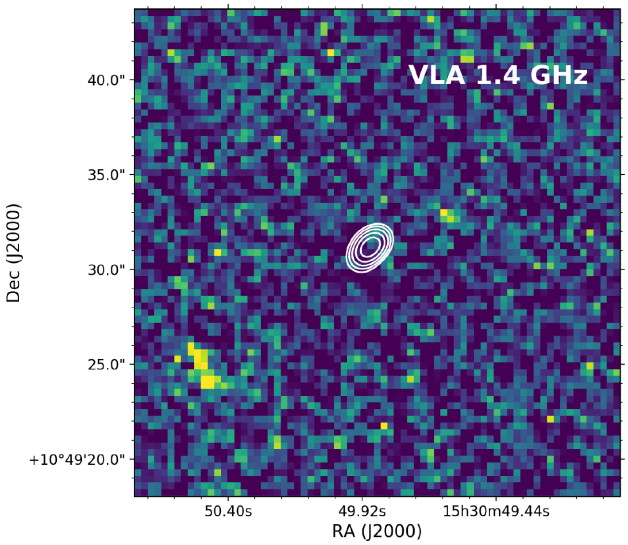

Figure 2. Stacked *y*, *J*, *H*, and *K* band image from the UKIDSS large-area Survey, with contours (starting from 0.5 mJy, in a geometric progression of $\sqrt{2}$) from the 1.4 GHz VLA map (Saxena et al. 2018) overplotted for TGSS J1530+1049. The radio source is compact and has an ultra-steep spectral index. A non-detection in the UKIDSS LAS *K* band down to a magnitude limit of 18.4 Vega (∼20.3 AB) made TGSS J1530+1049 a promising HzRG candidate and a prime target for spectroscopic follow-up.

compact radio morphology are in line with expectations of a high-redshift host galaxy and made TGSS J1530+1049 a prime candidate for follow-up spectroscopy.

3 OBSERVATIONS

3.1 Gemini GMOS spectroscopy

A long-slit spectrum of TGSS J1530+1049TGSS J1530+1049 was taken using GMOS on Gemini North on 28 April, 2017 (Program ID: GN-2017A-Q-8; PI: Overzier) using the filter GG455_G0305 and the R400_G5305 grating giving a wavelength coverage of 5400–10 800 Å and a resolution of roughly $R \sim 1500$. The central wavelength was set to 7000 Å. The total length of the slit was 300 arcsec and the slit width was chosen to be 1.5 arcsec so that it covers the entire radio emission footprint detected in the VLA image. As the host galaxy of the radio source was undetected in all available all-sky optical/IR surveys, we performed blind offsetting from a bright star, which ensures positional accuracy to within 0.1 arcsec, to the centroid of the radio emission. The VLA observations ensured sub-arcsec localization of the expected position of the host galaxy and the relatively large slit-width provided insurance against minor positional uncertainties. We took three exposures of 800 s each, giving a total of 2400 s of on-source exposure time. The standard star EG131 was observed for flux calibration.

We used the Gemini IRAF package for reducing the data, which includes the standard steps for optical spectrum reduction. Briefly, the bias frames were mean-stacked in a master bias which was subtracted from all other images acquired. Pixel-to-pixel sensitivity was corrected through the flat-field image taken during the day of the observations. The wavelength solution was derived from the arc lamp frame taken immediately after the science observations, and applied to the science frame and standard star. The 2D images were then combined in a single frame, rejecting possible cosmic rays. The sky lines were removed and flux calibration was achieved using the standard star spectrum.

A single emission line with a peak at 8170 Å and a spatial extent of ∼1 arcsec was detected in the reduced 2D spectrum at the expected position of the radio galaxy. No other line associated with this source was detected. No continuum was detected either bluewards or redwards of this line either. To ensure that the line detection is indeed real and not due to an artefact or contamination by cosmic rays, we looked at the individual frames, both raw and sky-subtracted, to ensure that the detection (although marginal) was present in each science frame. The three frames are shown in Fig. 3. The top panels show the raw frames and the bottom panels the sky-subtracted frames. The emission line is clearly present in all three frames, ensuring that the detection is real. The extracted 1D spectrum with a 1 arcsec aperture showing the detected emission line is shown in Fig. 4. We give details about line identification in Section 4.

3.2 Large Binocular Telescope NIR imaging

Imaging in the *J* and *Ks* bands using LUCI (formerly known as LUCIFER; Seifert et al. 2003) on the Large Binocular Telescope (LBT) was carried out in two separate runs, with the first on 1 February 2018 and the second on 11 May 2018 (Program ID 2017_2018_43; PI: Prandoni). The average seeing throughout the observations was 0.6 − 0.8 arcsec. In the first run, the on-source exposure time was 720 (12 × 60s) s in *J* (central wavelength of 1.247 microns) and 1200 (20 × 60s) s in *Ks* (central wavelength of 2.194 microns). In the second run, we obtained additional 3600 (30 × 120s) s in *J* and 3000 (50 × 60s) s in *Ks*, giving a total on-source exposure time of 4320 s in *J* band and 4200 s in *Ks* band. - The LUCI data reduction pipeline developed at INAF-OAR was used to perform the basic reduction such as dark subtraction, bad pixel masking, cosmic ray removal, flat fielding, and sky subtraction. Astrometric solutions for individual frames were obtained and the single frames were then resampled and combined using a weighted co-addition to form a deeper image. The $4' \times 4'$ field-of-view of LUCI contained many bright objects detected in both 2MASS and the UKIDSS Large Area

Downloaded from https://academic.oup.com/mnras/article-abstract/480/2/2733/5067277 by Royal Observatory Library user on 03 October 2018

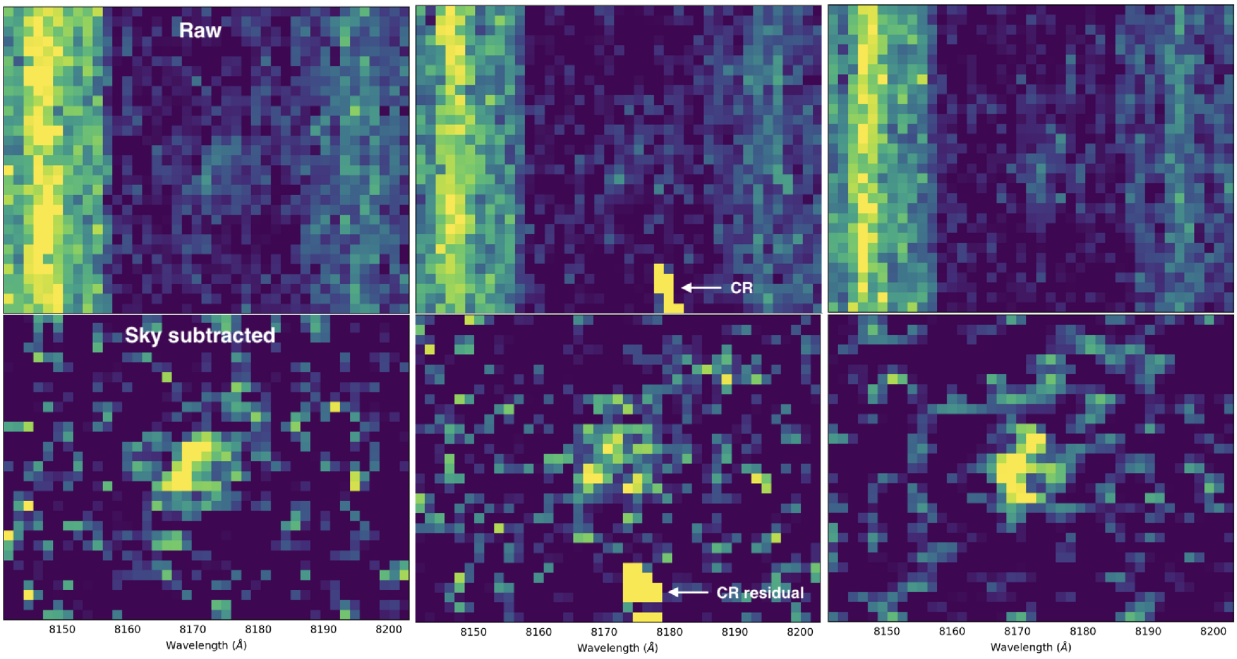

Figure 3. Raw (top panels) and sky subtracted (bottom panels) 2D frames shown for the three individual exposures taken using GMOS on Gemini. Traces of the emission line are visible in all three frames, ensuring that the detected line is real and not a consequence of cosmic rays or artefacts. There is some cosmic ray residual left over in the second frame but that does not contaminate the emission line signal.

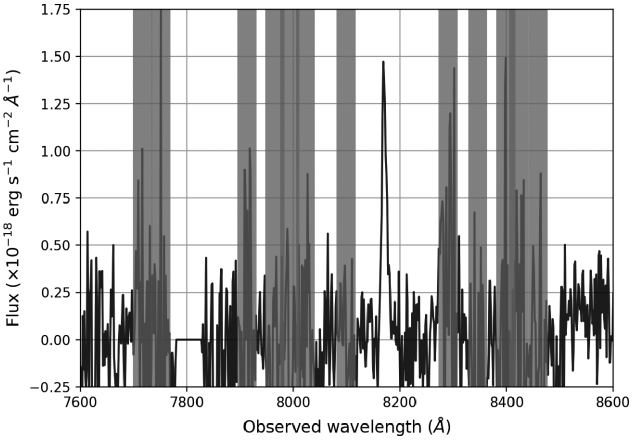

Figure 4. Extracted 1D spectrum showing the single emission line detection centred at 8170 Å from the GMOS 2D spectrum. No other line or continuum is detected. Shaded regions mark the presence of sky lines in the spectrum.

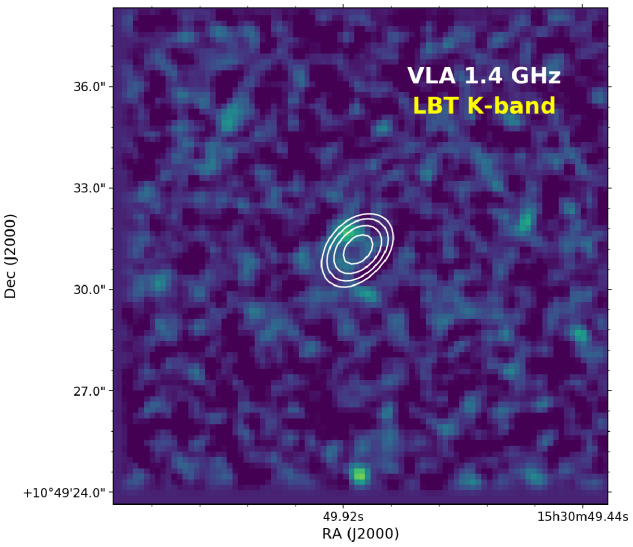

Figure 5. *K*-band image from the LBT, which has been smoothed with a 3 × 3 pixel Gaussian kernel, with radio contours (same as Fig. 2) from the VLA at 1.4-GHz overlaid. The measured magnitude at the radio position with a 1.5-arcsec aperture is fainter than the 3σ depth of the image, giving $K > 22.4$. When the image is smoothed, however, faint emission is visible around the peak of the radio emission. The magnitude limit is consistent with $z > 5$ following the $K - z$ relation for radio galaxies. For comparison, the $z = 5.2$ radio galaxy TN J09224 − 2201 has a K-band magnitude of 21.3 (van Breugel et al. 1999).

Survey, which were used to calibrate the photometry of the images in both bands.

The median and standard deviation of the background in both images was calculated by placing 5000 random apertures with a diameter of 1.5 arcsec. We measure 3σ depths of $J = 24.4$ and $Ks = 22.4$. Aperture photometry performed on both *J* and *Ks* (from here on we denote *Ks* as simply *K*) images using PHOTUTILS (Bradley et al. 2017) at the peak of the radio emission using an aperture of diameter 1.5 arcsec yield magnitudes that are lower than the 3σ depths in both images. Smoothing the *K*-band image with a 3 × 3 pixel Gaussian kernel reveals a faint source very close to the peak radio pixel, as shown in Fig. 5, but it is not entirely clear if this indeed is the host galaxy and there is no faint detection even in the smoothed *J*-band image. A summary of the observations is given in Table 1.

4 REDSHIFT DETERMINATION

We identify the single emission line detected in the GMOS spectrum as Lyα λ1216, giving a redshift of $z = 5.720 \pm 0.001$, which is shown in Fig. 6. Other plausible identifications of this emission line could be [O III] λ5007, giving a redshift of $z \approx 0.63$ or Hα λ6563 at

Downloaded from https://academic.oup.com/mnras/article-abstract/480/2/2733/5067277 by Royal Observatory Library user on 03 October 2018

Table 1. Observation log.

Telescope	Instrument	Date	Exp. time (sec)
Gemini N	GMOS long-slit	28-04-2017	2400 (3 × 800s)
LBT	LUCI J-band	01-02-2018	720 (12 × 60s)
		09-05-2018	3600 (30 × 120s)
	Total		4320
LBT	LUCI Ks-band	01-02-2018	1200 (20 × 60s)
		09-05-2018	3000 (50 × 60s)
	Total		4200

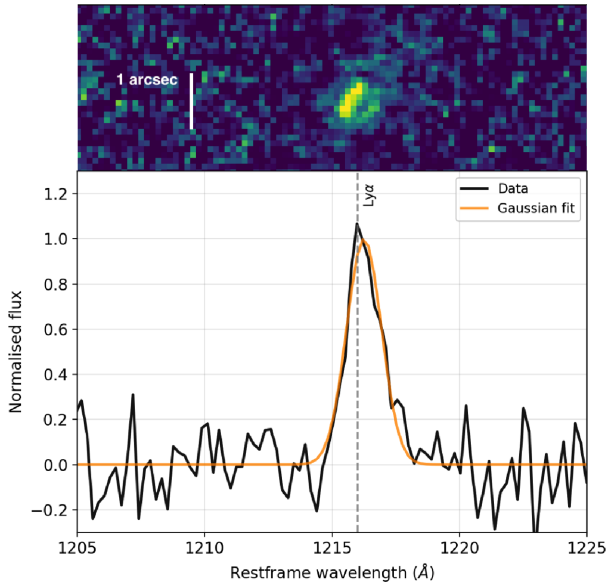

Figure 6. Rest-frame 1D spectrum showing the asymmetric Lyα line profile at a redshift of $z = 5.720$. Also shown is the best-fit Gaussian to the emission line. The peak of the fitted Gaussian is slightly redder than the peak of the line, suggesting asymmetry in the emission line. This is also clear from the excess towards the redder parts of the Gaussian. *Top:* The 2D GMOS spectrum showing the detected Lyα line. The spatial extent of the emission is roughly 1 arcsec, which is also the aperture size used to extract the 1D spectrum.

$z \approx 0.25$. These can be ruled out given the non-detection of other bright lines expected in the wavelength range covered. For example, if the observed line is [O III] at $z = 0.63$, then the [O II] λ3727 line would be observed at ∼6075 Å, unless the galaxy has a particularly high [O III]/[O II] ratio as in the case of very low-metallicity objects. An unresolved [O II] $\lambda\lambda$3726, 3729 doublet at a redshift of $z \approx 1.2$ could be a possibility, but the absence of other expected UV/optical lines common in AGN and radio galaxy spectra, such as C II] λ2326 or Mg II $\lambda\lambda$2797, 2803, which are, on average a factor of 2–4 times fainter than [O II] (De Breuck et al. 2001), makes this possibility unlikely. Another possibility could be C IV λ1549 giving $z = 4.27$, but this can be ruled out because in this case Lyα, which is often much brighter (for example, there are no radio galaxies in De Breuck et al. (2001) with Lyα flux lower than C IV λ1549 flux), would be expected at ∼6410 Å and we do not see any signs of an emission line in that region, which is free from bright sky lines.

We fit a Gaussian to the emission line (shown in Fig. 6) to measure an integrated line flux of $F_{Ly\alpha} = 1.6 \pm 0.6 \times 10^{-17}$ (error from 3σ noise level) erg s^{-1} cm^{-2}. The total measured Lyα luminosity is $L_{Ly\alpha} = 5.7 \pm 2.1 \times 10^{42}$ erg s^{-1}. The full width at half maximum (FWHM) after correcting for the instrumental FWHM is 370 ± 30 km s^{-1}. Since no continuum is detected in the spectrum (down to 1σ depth of 4.0×10^{-19} erg s^{-1} cm^{-2} Å^{-1}), we can only put a lower limit on the rest-frame equivalent width (EW) of the line, EW$_0$ >40 Å . Table 2 presents a summary of emission line measurements for TGSS J1530+1049.

Table 2. Spectroscopic redshift and emission line measurements for TGSS J1530+1049 through GMOS spectroscopy.

Property	Measurement
z_{spec}	5.720 ± 0.001
$F_{Ly\alpha}$	$1.6 \pm 0.6 \times 10^{-17}$ erg s^{-1} cm^{-2}
$L_{Ly\alpha}$	$5.7 \pm 2.1 \times 10^{42}$ erg s^{-1}
FWHM	370 ± 30 km s^{-1}
EW$_{obs}$	>40 Å

4.1 Skewness and equivalent width

To further confirm our redshift determination, we quantify the asymmetry of the emission line following the prescriptions laid out by Kashikawa et al. (2006), by calculating the S-statistic and the weighted skewness parameter. A measure of the skewness of the emission line is particularly useful when dealing with spectra with a single emission line and can help differentiate Lyα emission at high redshifts from [O II], [O III], or Hα emission from lower redshift galaxies (Rhoads et al. 2003; Kurk et al. 2004; Kashikawa et al. 2006). We measure the skewness $S = 0.31 \pm 0.14$ and the weighted skewness $S_w = 6.44 \pm 2.97$ Å , which are consistent with what is observed for confirmed Lyα emitters at high-redshift (Kashikawa et al. 2006, 2011; Matthee et al. 2017).

To check what possible values of skewness could be obtained from an unresolved [O II] doublet, we simulated the doublet with all possible ratios ($0.35 < j_{\lambda3729}/j_{\lambda3726} < 1.5$), convolved with the instrument resolution. We find that the skewness measured for the emission line seen in the spectrum ($S = 0.31$) is only possible for $j_{\lambda3729}/j_{\lambda3726} < 0.7$. These line ratios correspond to the high-electron-density regime when the line would be collisionally de-excited, and hence unlikely to be as strong as observed, with previous studies of the [O II] doublet in high-z galaxies (Steidel et al. 2014; Shimakawa et al. 2015; Sanders et al. 2016) also finding much higher line ratios on average. This helps drive the interpretation of the observed emission line more towards an Lyα at high-redshift.

Further, an EW >40 Å for an [O II] line originating from a presumably massive radio galaxy at $z \approx 1.2$ would be at the extreme end of the EW distribution (Bridge et al. 2015), including for radio-loud quasars (Kalfountzou et al. 2012). This EW value is also incompatible with the line ratios that would give rise to the observed skewness, as in regions of very high electron densities the [O II] line is expected to be weaker due to collisional de-excitation. Therefore, we can practically rule out the [O II] doublet as a possible identification of this emission line. An EW$_0$ >40 Å , however, is typical for Lyα emission seen in galaxies at $z \approx 5.7$ (see Kashikawa et al. 2011, for example) and generally consistent with the $z \sim 6$ galaxy population (De Barros et al. 2017).

4.2 K–z relation for radio galaxies

Finally, a strong indicator of a high-redshift nature of the host galaxy is the non-detection in K band down to a 3σ limiting magnitude of 22.4 (Fig. 5) using aperture photometry at the peak pixel of the

Downloaded from https://academic.oup.com/mnras/article-abstract/480/2/2733/5067277 by Royal Observatory Library user on 03 October 2018

Table 3. Comparison of Lyα emission line properties of TGSS J1530+1049 reported in this paper with some of the known radio galaxies at $z > 4$, and the much fainter radio galaxy at $z = 4.42$ (all marked as RG), in addition to several confirmed LAEs at $z \approx 5.7$ from the literature.

Name	z	$F_{Ly\alpha}$ ($\times 10^{-17}$ erg s^{-1} cm^{-2})	$L_{Ly\alpha}$ ($\times 10^{42}$ erg s^{-1})	FWHM$_{Ly\alpha}$ (km s^{-1})	Reference
TGSS J1530+1049	5.72	1.6	5.7	370	This work
TN J0924 − 2201 (RG)	5.19	3.4	9.6	1500	(van Breugel et al. 1999)
J163912.11 + 405236.5 (RG)	4.88	18.5	47.0	1040	(Jarvis et al. 2009)
VLA J123642 + 621331 (RG)	4.42	0.6	2.0	420	(Waddington et al. 1999)
LALA J142546.76 + 352036.3	5.75	1.6	6.7	360	(Rhoads et al. 2003)
S11 5236	5.72	14.9	9.1	200	(Lidman et al. 2012)
SDF J132344.8 + 272427	5.72	1.1	3.7	366	(Kashikawa et al. 2011)
HSC J232558+002557	5.70	3.6	12.6	373	(Shibuya et al. 2018)
SR6	5.67	7.6	25.0	236	(Matthee et al. 2017)

radio emission. For comparison, TN J0924 − 2201 at $z = 5.2$ has a magnitude of $K = 21.3 \pm 0.3$ and our measurement of $K > 22.4$ is consistent with $z > 5$ and helps rule out lower redshifts owing to the $K - z$ relation for radio galaxies (note that the luminosity and the spectral index rule out that it is a star-forming galaxy). We expand upon this point in Section 5.3. The additional non-detection in J band down to a 3σ limit of 24.3 further favours a high-redshift galaxy and supports the argument that the line we see is indeed Lyα and not [O II].

5 DISCUSSION

5.1 Emission line measurements

The Lyα luminosity and FWHM measured for TGSS J1530+1049 are lower than what is seen for typical HzRGs at $z > 4$ (see Spinrad, Dey & Graham 1995; De Breuck et al. 1999; van Breugel et al. 1999; Miley & De Breuck 2008, for examples) and more consistent with those measured for 'non-radio' Lyα-emitting galaxies (LAEs) at this redshift (Rhoads et al. 2003; Ouchi et al. 2008; Kashikawa et al. 2011; Lidman et al. 2012; Matthee et al. 2017). However, the FWHM for TGSS J1530+1049 is consistent with that of a very faint radio galaxy VLA J123642 + 621331, with a 1.4 GHz flux density of $S_{1.4\mathrm{GHz}} = 0.47$ mJy, discovered at $z = 4.424$ (Waddington et al. 1999). This galaxy has an FWHM of $\approx$420 km s^{-1} and an Lyα luminosity $\approx 2 \times 10^{42}$ erg s^{-1}, which is weaker than TGSS J1530+1049. VLA J123642 + 621331 is however, not detected in TGSS at 150 MHz down to a noise level of 3.5 mJy beam^{-1}, suggesting a relatively flat spectral index or a spectral turnover at low radio frequencies. We present some comparisons of the Lyα properties that we measure for TGSS J1530+1049 with other HzRGs at $z > 4$ and also non-radio LAEs at $z = 5.7$ in Table 3.

A statistical sample of radio galaxies at $z \sim 6$ is needed to understand whether they are more like LAEs at high-redshift or whether a majority of them continue being very different systems, surrounded by extremely overdense regions, and forming stars intensively. The relatively underluminous Lyα would be one signature of a significantly neutral intergalactic medium (IGM) during the late stages of the EoR. Weaker Lyα emission may also be caused by significant absorption in a cold and dusty medium surrounding the radio galaxy. The presence of cold gas and dust has been reported in many HzRGs, including TN J0924 − 2201 (see Klamer et al. 2005, for example) and dedicated observations to look for molecular gas and dust in a statistically significant sample of radio galaxies at $z > 5$ are required to better characterize their surrounding medium.

5.2 Radio properties

TGSS J1530+1049 has a flux density of 170 mJy at a frequency of 150 MHz and 7.5 mJy at 1.4 GHz (Saxena et al. 2018). Using the standard K-corrections in radio astronomy and assuming a constant spectral index of $\alpha = -1.4$, we calculate a rest-frame radio luminosity of $\log L_{150\mathrm{MHz}} = 29.1$ and $\log L_{1.4\mathrm{GHz}} = 28.2$ W Hz^{-1}, which places this source at the most luminous end of the radio luminosity function at this epoch (Saxena et al. 2017). For comparison, TN J0924 − 2201 has a K-corrected radio luminosity of $\log L_{1.4\mathrm{GHz}} = 29.3$ W Hz^{-1} using a spectral index of $\alpha = -1.6$ (van Breugel et al. 1999). TGSS J1530+1049 is close to an order of magnitude fainter than TN J09224 − 2201 at 1.4 GHz, but remains by far the brightest radio source observed this close to the end of the EOR.

The deconvolved angular size determined by Saxena et al. (2018) at 1.4 GHz for TGSS J1530+1049, which remains unresolved, is 0.6 arcsec, which translates to a linear size of 3.5 kpc. This size is smaller than the size of TN J0924 − 2201 (van Breugel et al. 1999) and in line with predictions at $z \sim 6$ from Saxena et al. (2017), as radio galaxies in the early Universe are expected to be young and very compact (Blundell et al. 1999). In Table 4, we compare the radio properties of TGSS J1530+1049 with all currently known radio galaxies at $z > 4$. This was done by querying the TGSS ADR1 catalogue to determine flux densities for all $z > 4$ radio galaxies at 150 MHz, which were then used to calculate radio powers using the standard K-corrections. We find that TGSS J1530+1049 is comparable to many of the $z > 4$ radio galaxies when looking at radio properties alone.

TGSS J1530+1049 has a spectral index of $\alpha_{1.4\ \mathrm{GHz}}^{150\ \mathrm{MHz}} = -1.4$, which is ultra-steep but flatter than TN J0924 − 2201 at $z = 5.19$, which was selected because of its spectral index of $\alpha_{1.4\ \mathrm{GHz}}^{365\ \mathrm{MHz}} = -1.6$. Interestingly, at lower radio frequencies, the spectral index of TN J0924 − 2201 appears to flatten dramatically. The 150-MHz flux density measured in TGSS (Intema et al. 2017) for TN J0924 − 2201 is 760 ± 76 mJy, giving a low-frequency spectral index $\alpha_{365\ \mathrm{MHz}}^{150\ \mathrm{MHz}} = -0.16$. If the spectral index were to be calculated only using the flux densities at frequencies of 150 MHz and 1.4 GHz, the inferred spectral index would be $\alpha_{1.4\ \mathrm{GHz}}^{150\ \mathrm{MHz}} = -1.06$, making it not strictly ultra-steep ($\alpha < -1.3$). This implies that in a search for ultra-steep spectrum radio sources using data at 150 MHz and 1.4 GHz, such as Saxena et al. (2018), TN J0924 − 2201 would be missed entirely. Indeed, an indication of a generally flatter spectral index at lower frequencies is visible in the spectral indices calculated for known $z > 4$ radio galaxies between frequencies of 150 MHz and 1.4 GHz in Table 4. A large majority of these radio sources were selected for having an ultra-steep

Downloaded from https://academic.oup.com/mnras/article-abstract/480/2/2733/5067277 by Royal Observatory Library user on 03 October 2018

Table 4. A comparison of the radio properties of TGSS J1530+1049 with other known radio galaxies at $z > 4$. Flux densities at 150 MHz are measured from the TGSS catalogue.

Name	z	S_{150} (mJy)	$\log L_{150}$ (W Hz^{-1})	S_{1400} (mJy)	α_{1400}^{150}	Size (kpc)	Reference
TGSS J1530+1049	5.72	170	29.1	7.5	−1.4	3.5	This work
TN J0924 − 2201	5.19	760	29.6	71.1	−1.1	7.4	(van Breugel et al. 1999)
J163912.11 + 405236.5	4.88	103	28.2	22.5	−0.7	–	(Jarvis et al. 2009)
RC J0311 + 0507	4.51	5981	30.3	500.0	−1.1	21.1	(Parijskij et al. 2014)
VLA J123642 + 621331	4.42	undetected	–	0.5	–	–	(Waddington et al. 1999)
6C 0140 + 326	4.41	860	29.4	91.0	−1.0	17.3	(Rawlings et al. 1996)
8C 1435 + 635	4.25	8070	30.4	497.0	−1.2	21.1	(Lacy et al. 1994)
TN J1123 − 2154	4.11	512	29.1	49.3	−1.0	5.5	(Reuland et al. 2004)
TN J1338 − 1942	4.10	1213	29.5	120.8	−1.0	37.8	(Reuland et al. 2004)

spectral index in a higher frequency range, but appear to have a flatter spectral index when calculated between 150 MHz and 1.4 GHz.

Spectral flattening or even a turnover at low radio frequencies is expected in radio galaxies at increasingly higher redshifts due to: a) Inverse Compton (IC) losses due to the denser cosmic microwave background that affect the higher frequencies and result in a steeper high-frequency spectral index, and b) free-free or synchrotron self-absorption due to the compact sizes of radio sources at high-redshifts that can lead to a turnover in the low-frequency spectrum (see Callingham et al. 2017, and references therein). Saxena et al. (2018) have reported evidence of flattening of the low-frequency spectral index in candidate HzRGs and observations at intermediate radio wavelengths for sources like TGSS J1530+1049 are essential to measure spectral flattening and constrain various energy-loss mechanisms that dominate the environments of radio galaxies in the early Universe. Additionally, search techniques for radio galaxies at even higher redshifts could be refined by possibly using radio colours instead of a simple ultra-steep spectral index selection. The LOFAR Two Metre Sky Survey (Shimwell et al. 2017, Shimwell et al. submitted) will eventually provide in-band spectral indices at 150 MHz and could potentially be used to identify HzRG candidates more efficiently.

We also draw attention towards the radio galaxy J163912.11 + 405236.5 at $z = 4.88$ (Jarvis et al. 2009), that has a spectral index of $\alpha_{1.4\,\mathrm{GHz}}^{325\,\mathrm{MHz}} = -0.75$ and is not an ultra-steep spectrum radio source. Interestingly, there is evidence of spectral flattening at lower frequencies with a 150-MHz flux density of 103.5 mJy, giving a spectral index $\alpha_{325\,\mathrm{MHz}}^{150\,\mathrm{MHz}} = -0.56$, which is flatter than that at higher frequencies. This source was targeted for spectroscopic follow-up owing to the faintness of its host galaxy at 3.6 μm. The very faint radio galaxy VLA J123642 + 621331 at $z = 4.42$ (Waddington et al. 1999) is also not strictly an ultra-steep spectrum source at high radio frequencies ($\alpha_{4.8\,\mathrm{GHz}}^{1.4\,\mathrm{GHz}} = -0.94$) and is too faint to be detected in TGSS. This source was also selected based on its optical and infrared faintness, suggesting that a considerable fraction of HzRGs may not be ultra-steep at all and therefore, be missed in samples constructed using the ultra-steep spectrum selection technique.

Indeed, Ker et al. (2012) have shown that selecting infrared-faint radio sources (IFRS) could be more efficient at isolating HzRGs from large samples when compared to radio selection alone. This has been confirmed observationally through many previous studies (Norris et al. 2006; Collier et al. 2014; Herzog et al. 2014; Maini et al. 2016; Singh et al. 2017). However, the caveat is that deep infrared photometry over large sky areas is required to effectively implement such a selection, which can be expensive. The recently concluded UKIRT Hemisphere Survey (UHS; Dye et al. 2018) has the potential to be extremely useful in the identification of promising HzRG candidates in the Northern Hemisphere, particularly from the LOFAR surveys (Shimwell et al. 2017, Shimwell et al. submitted), as a combination of a relaxed spectral index steepness criterion and infrared-faintness could be more effective at isolating HzRGs.

5.3 Stellar mass limits

The non-detection of the host galaxy down to a 3σ depth of $K = 22.4$ can be used to set limits on the stellar mass for TGSS J1530+1049 using simple stellar population synthesis modelling. To do this, we make use of the PYTHON package SMPY,[1] which is designed for building composite stellar populations in an easy and flexible manner, allowing for synthetic photometry to be produced for single or large suites of models (see Duncan & Conselice 2015). To build stellar populations, we use the Bruzual & Charlot (2003) model with a Chabrier (2003) initial mass function (IMF) and solar metallicity (Willott et al. 2003), a formation redshift $z_f = 25$, and assume a maximally old stellar population that has been forming stars at a constant rate (Lacy, Bunker & Ridgway 2000). We follow the Calzetti et al. (2000) law for dust attenuation and use values of $A_v = 0.15$ (moderate extinction) and 0.5 mag (dusty), which are commonly seen in massive galaxies at $5 < z < 6$ (McLure et al. 2006). The synthetic photometry is produced for different stellar masses, which we then convolve with the K-band filter to calculate apparent K magnitudes over a redshift range $0 - 7$.

The K magnitude limit for TGSS J1530+1049 fits well with a stellar mass limit of $M_{\mathrm{stars}} < \sim 10^{10.25}$ M$_\odot$ for $A_v = 0.15$ mag, and $M_{\mathrm{stars}} < \sim 10^{10.5}$ for $A_v = 0.5$ mag. We note here that thanks to the excellent K-band observations ($0.6 - 0.8$ arcsec), and since at $z \sim 6$ the host galaxy is expected to be small, any aperture correction is only expected to be at the level of a few tenths of a magnitude at most, or $0.1 - 0.2$ in the logarithmic stellar mass, which is smaller than the uncertainty from dust extinction corrections.

We find that the stellar mass limits we infer are in agreement with the J-band 3σ limit from LBT. The photometry predicted by the models in the optical bands from PS1 (g, r, i, z, y) is also consistent with the non-detections that we report. This stellar mass limit places TGSS J1530+1049 towards the $>M*$ end of the galaxy stellar mass function at $z \sim 6$ (see Duncan et al. 2014, for example). For comparison, we show the apparent K-band magnitudes of other radio galaxies in the literature, taken from the 3CRR, 6CE, 6C*, and 7C−I/II/III samples (Willott et al. 2003), in Fig. 7. Also shown

[1] https://github.com/dunkenj/smpy

Downloaded from https://academic.oup.com/mnras/article-abstract/480/2/2733/5067277 by Royal Observatory Library user on 03 October 2018

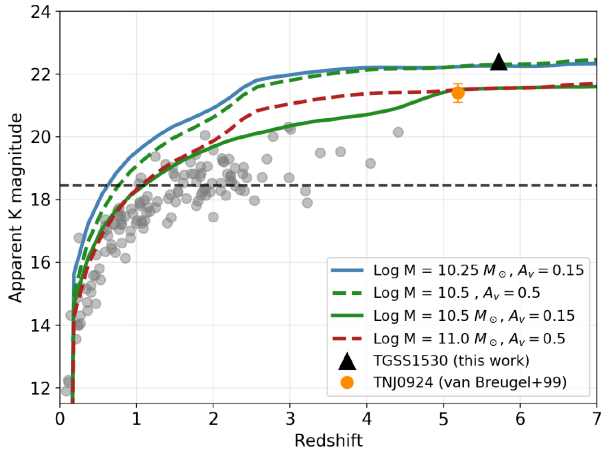

Figure 7. The '$K - z$' diagram for radio galaxies, showing stellar mass limits derived from stellar population synthesis modelling for TGSS J1530+1049 (black triangle). The K-band 3σ limit gives $M_{\rm stars} < 10^{10.25}$ $M_\odot$ for $A_v = 0.15$ mag, and $M_{\rm stars} < 10^{10.5}$ for $A_v = 0.5$ mag. Also shown are K-band magnitudes and redshifts for known radio galaxies in the literature (grey points; see text), with TN J0924 − 2201 at $z = 5.19$ (orange circle). The K-band limits for TGSS J1530+1049 further help exclude lower redshift measurements from incorrect line identification.

is the K magnitude for TN J09224 − 2201 at $z = 5.2$ (van Breugel et al. 1999), which is best fit with a stellar mass of $10^{10.5}$ $M_\odot$ for $A_v = 0.15$ mag and 10^{11} $M_\odot$ for $A_v = 0.5$ mag.

We also show the K-band magnitude limit for the UKIDSS LAS as a dashed black line in Fig. 7. TGSS J1530+1049 was initially selected due to its non-detection in LAS. However, these magnitude limits alone were not sufficient to constrain the very high-redshift nature of the host galaxy. With deeper LBT observations in K band, we show that TGSS J1530+1049 follows the trend in the $K - z$ plot for radio galaxies. It is also clear that a low-redshift solution that would arise if the detected emission line in Section 4 is not Lyman alpha (for example, $z \approx 1.2$ if the line is [O II]) would be hard to explain using galaxy evolution models with the inputs and assumptions outlined above and those generally used to model radio galaxy spectra (Overzier et al. 2009).

A stellar mass limit of $M_\star < 10^{10.5}$ $M_\odot$ for TGSS J1530+1049 (based on the outlined assumptions) is almost an order of magnitude lower than the sample of radio galaxies studied by Rocca-Volmerange et al. (2004), where the highest stellar masses are seen for radio galaxies in the redshift range 2 − 4. This suggests that TGSS J1530+1049 is still evolving and is in the process of building up its stellar mass. This interpretation is in line with TGSS J1530+1049 being a relatively young radio galaxy owing to its small radio size, and lower stellar masses may be expected from radio galaxies close to or into the epoch of reionization. Robust detections at optical and infrared wavelengths are required to properly characterize the galaxy spectral energy distribution in order to understand better the star formation history of TGSS J1530+1049.

6 CONCLUSIONS

In this paper, we have presented the discovery of the highest redshift radio galaxy, TGSS J1530+1049, at $z = 5.72$. The galaxy was initially selected at 150 MHz from TGSS (Saxena et al. 2018) and was assigned a high priority for spectroscopic follow-up owing to its compact morphology and faintness at optical and near-infrared wavelengths. The conclusions of this study are listed below:

(i) Long-slit spectroscopy centred at the radio position of the source revealed an emission line at 8170 Å, which we identify as Lyman alpha at $z = 5.720$. We rule out alternative line IDs owing to the absence of other optical/UV lines in the spectrum, the asymmetrical nature of the emission line characteristic of Lyman alpha at high redshifts that we quantify using the skewness parameter, and the high observed equivalent width of the emission line.

(ii) Deep J and K band imaging using the Large Binocular Telescope led to no significant detection of the host galaxy down to 3σ limits of $K > 22.4$ and $J > 24.4$. The limits in K can be used as an additional constraint on the redshift, owing to the relation that exists between K-band magnitude and redshift of radio galaxies. The magnitude limit is consistent with $z > 5$, practically ruling out a redshift of $z \approx 1.2$ that would be expected if the emission line were an unresolved [O II] λλ3726, 3729 doublet, which is the most likely alternative line identification.

(iii) The emission line is best fitted with a skewed Gaussian, giving an integrated line flux of $F_{Ly\alpha} = 1.6 \times 10^{-17}$ erg s^{-1} cm^{-2}, an Lyα luminosity of 5.7×10^{42} erg s^{-1}, an equivalent width of EW >40 Å, and an FWHM of 370 km s^{-1}. These values are more consistent with those observed in non-radio Lyman alpha emitting galaxies at this redshift and much lower than those corresponding to typical radio galaxies at $z > 4$.

(iv) The radio luminosity calculated at 150 MHz is $\log L_{150} = 29.1$ W Hz^{-1}, which places it at the most luminous end of the radio luminosity function at this epoch. The deconvolved angular size is 3.5 kpc, which is in line with the compact morphologies expected at high-redshifts. We find that the radio properties of TGSS J1530+1049 are comparable to other known radio galaxies at $z >$ 4 but the compact size suggests that it is a radio galaxy in an early phase of its evolution. A joint study of the Lyα halo and the radio size of this source may provide one of the earliest constraints on the effects of radio-mode feedback.

(v) We use the K band limit to put constraints on the stellar mass estimate using simple stellar population synthesis models. Assuming a constant star formation history and a maximally old stellar population, we derive a stellar mass limit of $M_{\rm stars} < \sim 10^{10.25}$ $M_\odot$ for $A_v = 0.15$ mag, and $M_{\rm stars} < \sim 10^{10.5}$ for $A_v = 0.5$ mag. These limits are almost an order of magnitude lower than typical radio galaxy masses in the redshift range 2 − 3 and suggest that TGSS J1530+1049 may still be in the process of assembling its stellar mass, which is in line with it being a relatively young radio galaxy.

An effective application of deep radio surveys covering very large areas on the sky has been demonstrated by this discovery of the first radio galaxy at a record distance after almost 20 years. With the more sensitive, large-area surveys currently underway with LOFAR (LoTSS; Shimwell et al. 2017, Shimwell et al. submitted), there is potential to push searches for radio galaxies to even higher redshifts. Discovery of even a single bright radio galaxy at $z > 6$ would open up new ways to study the EOR in unparalleled detail, through searches for the 21-cm absorption features left behind by the neutral hydrogen that pervaded the Universe at high-redshifts.

ACKNOWLEDGEMENTS

The authors thank the referee for useful comments and suggestions. AS would like to thank Jorryt Matthee, David Sobral, Reinout van Weeren, and Nobunari Kashikawa for fruitful discussions. AS, HJR, and KJD gratefully acknowledge support from the European Research Council under the European Unions Seventh Framework

Downloaded from https://academic.oup.com/mnras/article-abstract/480/2/2733/5067277 by Royal Observatory Library user on 03 October 2018

Programme (FP/2007-2013)/ERC Advanced Grant NEWCLUSTERS-321271. RAO and MM received support from CNPq (400738/2014-7, 309456/2016-9) and FAPERJ (202.876/2015). PNB is grateful for support from STFC via grant ST/M001229/1. IP acknowledges funding from the INAF PRIN-SKA 2017 project 1.05.01.88.04 (FORECaST).

This paper is based on results from observations obtained at the Gemini Observatory, which is operated by the Association of Universities for Research in Astronomy, Inc., under a cooperative agreement with the NSF on behalf of the Gemini partnership: the National Science Foundation (United States), the National Research Council (Canada), CONICYT (Chile), Ministerio de Ciencia, Tecnología e Innovación Productiva (Argentina), and Ministério da Ciência, Tecnologia, Inovação e Comunicações (Brazil). This paper also contains data from the Large Binocular Telescope (LBT), an international collaboration among institutions in the United States, Italy, and Germany. LBT Corporation partners are: The University of Arizona on behalf of the Arizona University System; Istituto Nazionale di Astrofisica, Italy; LBT Beteiligungsgesellschaft, Germany, representing the Max-Planck Society, the Astrophysical Institute Potsdam, and Heidelberg University; The Ohio State University, and The Research Corporation, on behalf of The University of Notre Dame, University of Minnesota, and University of Virginia.

This work has made extensive use of IPYTHON (Pérez & Granger 2007), ASTROPY (Astropy Collaboration et al. 2013), APLPY (Robitaille & Bressert 2012), MATPLOTLIB (Hunter 2007) and TOPCAT (Taylor 2005). This work would not have been possible without the countless hours put in by members of the open-source developing community all around the world.

REFERENCES

Afonso J. et al., 2011, ApJ, 743, 122
Alam S. et al., 2015, ApJS, 219, 12
Astropy Collaboration et al., 2013, A&A, 558, A33
Bañados E. et al., 2015, ApJ, 804, 118
Bañados E., Carilli C., Walter F., Momjian E., Decarli R., Farina E. P., Mazzucchelli C., Venemans B. P., 2018, ApJ, 861, L14
Best P. N. et al., 1998, MNRAS, 301, L15
Blundell K. M., Rawlings S., Willott C. J., 1999, AJ, 117, 677
Bradley L. et al., 2017, astropy/photutils: v0.4,
Bridge J. S. et al., 2015, ApJ, 799, 205
Bruzual G., Charlot S., 2003, MNRAS, 344, 1000
Callingham J. R. et al., 2017, ApJ, 836, 174
Calzetti D., Armus L., Bohlin R. C., Kinney A. L., Koornneef J., Storchi-Bergmann T., 2000, ApJ, 533, 682
Carilli C. L., Harris D. E., Pentericci L., Röttgering H. J. A., Miley G. K., Kurk J. D., van Breugel W., 2002a, ApJ, 567, 781
Carilli C. L., Gnedin N. Y., Owen F., 2002b, ApJ, 577, 22
Chabrier G., 2003, PASP, 115, 763
Chambers K. C. et al., 2016, preprint (arXiv:1612.05560)
Ciardi B. et al., 2015, MNRAS, 453, 101
Collier J. D. et al., 2014, MNRAS, 439, 545
De Barros S. et al., 2017, A&A, 608, A123
De Breuck C., van Breugel W., Minniti D., Miley G., Röttgering H., Stanford S. A., Carilli C., 1999, A&A, 352, L51
De Breuck C., van Breugel W., Röttgering H. J. A., Miley G., 2000, A&AS, 143, 303
De Breuck C. et al., 2001, AJ, 121, 1241
De Breuck C. et al., 2010, ApJ, 725, 36
Dewdney P. E., Hall P. J., Schilizzi R. T., Lazio T. J. L. W., 2009, IEEE Proceedings, 97, 1482
Duncan K., Conselice C. J., 2015, MNRAS, 451, 2030
Duncan K. et al., 2014, MNRAS, 444, 2960
Dunlop J. S., Peacock J. A., 1990, MNRAS, 247, 19
Dye S. et al., 2018, MNRAS, 473, 5113
Ewall-Wice A., Dillon J. S., Mesinger A., Hewitt J., 2014, MNRAS, 441, 2476
Furlanetto S. R., Loeb A., 2002, ApJ, 579, 1
Hatch N. A. et al., 2011, MNRAS, 410, 1537
Herzog A., Middelberg E., Norris R. P., Sharp R., Spitler L. R., Parker Q. A., 2014, A&A, 567, A104
Hunter J. D., 2007, Computing In Science & Engineering, 9, 90
Intema H. T., Jagannathan P., Mooley K. P., Frail D. A., 2017, A&A, 598, A78
Ishwara-Chandra C. H., Sirothia S. K., Wadadekar Y., Pal S., Windhorst R., 2010, MNRAS, 405, 436
Jarvis M. J., Rawlings S., Eales S., Blundell K. M., Bunker A. J., Croft S., McLure R. J., Willott C. J., 2001, MNRAS, 326, 1585
Jarvis M. J., Teimourian H., Simpson C., Smith D. J. B., Rawlings S., Bonfield D., 2009, MNRAS, 398, L83
Kalfountzou E., Jarvis M. J., Bonfield D. G., Hardcastle M. J., 2012, MNRAS, 427, 2401
Kashikawa N. et al., 2006, ApJ, 648, 7
Kashikawa N. et al., 2011, ApJ, 734, 119
Ker L. M., Best P. N., Rigby E. E., Röttgering H. J. A., Gendre M. A., 2012, MNRAS, 420, 2644
Klamer I. J., Ekers R. D., Sadler E. M., Weiss A., Hunstead R. W., De Breuck C., 2005, ApJ, 621, L1
Kurk J. D., Cimatti A., di Serego Alighieri S., Vernet J., Daddi E., Ferrara A., Ciardi B., 2004, A&A, 422, L13
Lacy M. et al., 1994, MNRAS, 271, 504
Lacy M., Bunker A. J., Ridgway S. E., 2000, AJ, 120, 68
Lawrence A. et al., 2007, MNRAS, 379, 1599
Lidman C., Hayes M., Jones D. H., Schaerer D., Westra E., Tapken C., Meisenheimer K., Verhamme A., 2012, MNRAS, 420, 1946
Lilly S. J., Longair M. S., 1984, MNRAS, 211, 833
Mack K. J., Wyithe J. S. B., 2012, MNRAS, 425, 2988
Maini A., Prandoni I., Norris R. P., Spitler L. R., Mignano A., Lacy M., Morganti R., 2016, A&A, 596, A80
Matthee J., Sobral D., Darvish B., Santos S., Mobasher B., Paulino-Afonso A., Röttgering H., Alegre L., 2017, MNRAS, 472, 772
McLure R. J. et al., 2006, MNRAS, 372, 357
Miley G., De Breuck C., 2008, A&A Rev., 15, 67
Miley G. K. et al., 2004, Nature, 427, 47
Momjian E., Carilli C. L., Bañados E., Walter F., Venemans B. P., 2018, ApJ, 861, 86
Morabito L. K. et al., 2017, MNRAS, 469, 1883
Norris R. P. et al., 2006, AJ, 132, 2409
Orsi Á. A., Fanidakis N., Lacey C. G., Baugh C. M., 2016, MNRAS, 456, 3827
Ouchi M. et al., 2008, ApJS, 176, 301
Overzier R. A. et al., 2009, ApJ, 704, 548
Parijskij Y. N. et al., 2014, MNRAS, 439, 2314
Pentericci L. et al., 2000, A&A, 361, L25
Pérez F., Granger B. E., 2007, Computing in Science and Engineering, 9, 21
Rawlings S., Lacy M., Blundell K. M., Eales S. A., Bunker A. J., Garrington S. T., 1996, Nature, 383, 502
Reuland M., Röttgering H., van Breugel W., De Breuck C., 2004, MNRAS, 353, 377
Rhoads J. E. et al., 2003, AJ, 125, 1006
Rigby E. E., Best P. N., Brookes M. H., Peacock J. A., Dunlop J. S., Röttgering H. J. A., Wall J. V., Ker L., 2011, MNRAS, 416, 1900
Rigby E. E., Argyle J., Best P. N., Rosario D., Röttgering H. J. A., 2015, A&A, 581, A96
Robitaille T., Bressert E., 2012, APLpy: Astronomical Plotting Library in Python, Astrophysics Source Code Library
Rocca-Volmerange B., Le Borgne D., De Breuck C., Fioc M., Moy E., 2004, A&A, 415, 931
Röttgering H. J. A., Lacy M., Miley G. K., Chambers K. C., Saunders R., 1994, A&AS, 108
Röttgering H., Daddi E., Overzier R., Wilman R., 2003, New A Rev., 47, 309

Downloaded from https://academic.oup.com/mnras/article-abstract/480/2/2733/5067277 by Royal Observatory Library user on 03 October 2018

Sanders R. L. et al., 2016, ApJ, 816, 23
Saxena A., Röttgering H. J. A., Rigby E. E., 2017, MNRAS, 469, 4083
Saxena A. et al., 2018, MNRAS, 475, 5041
Seifert W. et al., 2003, in Iye M., Moorwood A. F. M., eds, Proc. SPIEVol. 4841, Instrument Design and Performance for Optical/Infrared Ground-based Telescopes. pp. 962–973,
Shibuya T. et al., 2018, PASJ, 70, S15
Shimakawa R. et al., 2015, MNRAS, 451, 1284
Shimwell T. W. et al., 2017, A&A, 598, A104
Singh V., Wadadekar Y., Ishwara-Chandra C. H., Sirothia S., Sievers J., Beelen A., Omont A., 2017, MNRAS, 470, 4956
Smith D. J. B. et al., 2016, in Reylé C., Richard J., Cambrésy L., Deleuil M., Pécontal E., Tresse L., Vauglin I., eds, SF2A-2016: Proceedings of the Annual meeting of the French Society of Astronomy and Astrophysics. pp. 271–280
Spinrad H., Dey A., Graham J. R., 1995, ApJ, 438, L51
Steidel C. C. et al., 2014, ApJ, 795, 165
Swarup G., Ananthakrishnan S., Kapahi V. K., Rao A. P., Subrahmanya C. R., Kulkarni V. K., 1991, Current Science, 60, 95
Taylor M. B., 2005, in Shopbell P., Britton M., Ebert R., eds, Astronomical Society of the Pacific Conference Series Vol. 347, Astronomical Data Analysis Software and Systems XIV. p. 29
Tingay S. J. et al., 2013, PASA, 30, e007
van Breugel W., De Breuck C., Stanford S. A., Stern D., Röttgering H., Miley G., 1999, ApJ, 518, L61
van Haarlem M. P. et al., 2013, A&A, 556, A2
Venemans B. P. et al., 2002, ApJ, 569, L11
Waddington I., Windhorst R. A., Cohen S. H., Partridge R. B., Spinrad H., Stern D., 1999, ApJ, 526, L77
Willott C. J., Rawlings S., Blundell K. M., Lacy M., Eales S. A., 2001, MNRAS, 322, 536
Willott C. J., Rawlings S., Jarvis M. J., Blundell K. M., 2003, MNRAS, 339, 173
Wright E. L. et al., 2010, AJ, 140, 1868
Xu Y., Chen X., Fan Z., Trac H., Cen R., 2009, ApJ, 704, 1396

This paper has been typeset from a TEX/LATEX file prepared by the author.

Downloaded from https://academic.oup.com/mnras/article-abstract/480/2/2733/5067277 by Royal Observatory Library user on 03 October 2018